Efficiency improvement of thin film solar cell using silver pyramids array and antireflective layer

Abu S.M. Mohsin [*], Sujoy Mondal, Monica Mobashera, Afrida Malik, Maliha Islam, Maisha Rubaiat

Department of Electrical and Electronic Engineering, Nanotechnology, IoT and Applied Machine Learning Research Group Brac University, 66 Mohakhali, Dhaka, Bangladesh

ARTICLE INFO

ABSTRACT

In recent years, plasmonics has been widely employed to improve light trapping in solar cells. Silver nanospheres have been used in several research works to improve the capability of solar absorption. In this paper, we use silver pyramid-shaped nanoparticles, a noble plasmonic nanoparticle, inside thin-film silicon and InP solar cells to increase light absorption compared to previously published topologies. The proposed structure consists of a TiO_2 pyramid structure placed at the top of the surface working as an anti-reflective layer, silicon/indium phosphate as an absorption layer, silver pyramid-shaped nanoparticles incorporated inside the absorption layer, and an aluminum reflecting layer at the bottom. In this research, we used finite difference time domain (FDTD) simulation to model the thin-film solar cell (TFSC). Optimizing the shape and placement of the silver pyramids, we have achieved an efficiency of 17.08% and 18.58% using silicon and InP as the absorbing layers respectively, which is significantly better than previously reported studies. The open-circuit voltages are 0.58 V and 0.92 V respectively, which is the highest among other configurations. To conclude, the findings of this study laid the foundation to create an efficient thin-film solar cell utilizing the light-trapping mechanism of noble plasmonic nanoparticles.

1. Introduction

One of the substantial challenges of today's society is to have the supply of cost-effective and environment-friendly energy that can fulfill the demand of the ever-growing population. The photovoltaic energy source can meet this demand as the total radiation which hits this earth is 1.7×10^5 TW (TW), and we use only 15 TW [1]. However, the cost per watt is comparatively high in photovoltaic modules concerning other renewable and non-renewable sources, and this is one of the driving forces which motivates us to establish more efficient and cost-effective solar cells.

Sunlight is transformed into electricity-generating power when it rebounds on a solar cell. Semiconductors are employed in the p-n junction configuration for solar energy conversion [2]. Both single-junction and multiple-junction solar cells have been investigated over the years. The highest theoretical efficiency of a single-junction solar cell is known to be 33.16%, according to analytical investigation [3]. The effectiveness of junctions is 86.8% for an unlimited number of them [4]. However, compared to the theoretically allowed value, the maximum recorded efficiency utilizing thin film silicon solar cells is substantially lower. There have been several

---

studies on plasmonic [5–10], organic [11,12], dye-sensitized [13–16], and photonic crystals [17–20] to improve solar cell efficiency.

Thin-film solar cells have drawn a lot of interest despite having relatively poor efficiency when compared to other structures because of their affordable production [19,21,and22]]. The fundamental cause of insufficient efficiency is Si's extremely low absorption at longer wavelengths. To increase overall efficiency, it is necessary to improve optical (light) absorption and electrical current generation in solar cells. Several schemes [5–10,23] have been put out to enhance absorption based on the light-trapping process. Solar cell efficiency can be significantly increased by using effective scattering of light incorporating nanophotonic components like metal nanoparticles inside the absorbing layer. Reducing unwanted back reflections using nanotextured anti-reflection coatings can also increase efficiency [10,24,25]. Other prevalent strategies for increasing absorption include selecting the proper transparent conducting film [26], radiative cooling [27], encouraging visible spectrum light scattering [28–30], rear surface passivation [31], antireflective coatings and textures [32], and choosing the proper thin-film materials [33].

Both light scattering and light absorption are possible as a result of the resonant interaction of light with nanoparticles (NPs) at plasmonic resonance. The advantage of scattering comes from the light's longer travel inside photovoltaic material, which enhances the likelihood that scattered photons will be absorbed and produce photocurrent. In contrast, light trapping caused by parasitic absorpton, or absorption that takes place inside the NPs, can significantly reduce the overall photocurrent amplification that can be achieved in a solar cell [34–36]. The NPs for Photovoltaic applications must be properly engineered and designed in order to optimize the scattering and mitigate the parasitic losses over the spectral range crucial for light trapping, as the optical properties of plasmonic NPs rely strongly on their size, shape, and local environment [37].

Although several materials have been tried as plasmonic NPs, silver seems to be the most promising one because of its high radiative efficiency and low imaginary permittivity in the visible and near-infrared spectrum. The main role of nanoparticles inside the absorbing layer is to increase the path length traveled by the incoming light to increase absorption. Both Gold and Silver particles are capable of producing this effect using plasmonic effects. Differently-shaped silver and gold nanoparticles (nanospheres, nanorods, nanocubes) have been investigated in some previous studies [7,8,38–40,41] to explore their effect on light absorption in thin-film silicon solar cells. The maximum efficiency reported using silver nanospheres is 16.18% and gold nanorods is 16.23% [8,39]. The novelty of this work lies in the exploration of how pyramid-shaped nanoparticles inside the silicon absorption layer can increase the optical path length within the solar cell, which has not been investigated yet, producing a solar cell that is incredibly efficient. Simulation has been performed using both gold and silver nanoparticles producing almost similar results making us decide to choose Silver as the ultimate choice of materials for reducing the production cost. The reflection from the front surface of solar cells is a complicated issue that prevents efficient energy harvesting. Different anti-reflection surface structures have been investigated over the years to prevent reflection from the upper surface and redirect the ray inside the absorption layer. Grating structure on top of the absorption layer with different materials such as Silicon [42], Silver [43], and Gold [44] is a common technique for absorption improvement. The major drawbacks of grating structures are lower angular coverage and dependence on polarization of the incoming light. The most promising way of reducing reflection is the use of pyramid-shaped structures above the absorption layer, which can collect light from a wider angle and works both for TE and TM waves. TiO$_2$ is the choice of material for use as the antireflection pyramid layer because of its high refractive index and high transparency in the visible wavelength, which helps to absorb light waves from a wider angle and redirect it inside the absorption layer [45]. Besides, solar cells need to be very stable under exposure to sunlight and moisture and TiO$_2$ is a good choice to meet these criteria. Additionally, a layer of Aluminium reflecting material is positioned at the base of the surface to reduce energy loss through non-absorption inside the cell. With all of these features, we were capable of attaining an efficiency of 17.08%, which is 6% better compared to the reported thin film solar cells. The same characteristics have been adopted in InP thin film solar cells as well, and the efficiency has increased up to 18.58%.

2. Methodology

Theory: The length of the optical path and absorption coefficient play a vital role in determining how much energy is being absorbed by the semiconductor material. A semiconductor has a finite absorption coefficient therefore it can absorb all the incoming light. However, inside dielectric environments, certain light rays are reflected from various solar cell surfaces. To overcome these issues several approaches have been proposed, such as texturing the top surface like a pyramid, use of a rear mirror, or placing irregular patterns in the upper and rear surfaces of the solar cell.

Also to absorb more solar spectrum in the range of 600 nm–1100 nm, larger thickness (e.g. 180–300 μm) wafer-based crystalline Si cells have been introduced. However, the problem remains unresolved as the diffusion length of minority carriers is several times higher than the thickness of the material.

Recently this problem has been resolved by introducing plasmonic nanoparticles on either the back or front of an absorbing layer utilizing a light-trapping mechanism. Following this process, the path length can be increased within the absorption layer [46] which will eventually increase the scattering efficiency.

When a metal nanoparticle is placed on top of a dielectric or semiconductor at the interface of a metal-dielectric surface plasmon polariton (SPP) is created. Surface plasmons are coherent oscillations of free electrons on an interface of metal (negative) and dielectric (positive) with opposite signs. The surface plasmon wave vector (K_{sp}) can be described as equation no 1 below.

$$K_{sp} = \frac{\omega}{c\sqrt{\frac{\varepsilon_s.\varepsilon_m}{\varepsilon_s+\varepsilon_m}}} \tag{1}$$

where ϵ_s = dielectric function of dielectric and ϵ_m = dielectric function of the metal.

Table-1

Absorption cross-sections for different nanoparticles.

Structures	Absorption Cross-Section at 500 nm wavelength (m^2)	Absorption Cross-Section at 600 nm wavelength (m^2)	Absorption Cross-Section at 700 nm wavelength (m^2)
Nanospheres 50 nm Radius	1.8×10^{-14}	3.2×10^{-14}	1.9×10^{-14}
Nanorods 80 nm Length, 40 nm diameter	3×10^{-14}	5.6×10^{-14}	2.1×10^{-14}
Nanocubes length 120 nm	7.6×10^{-14}	2.12×10^{-13}	8×10^{-14}
Nanopyramids 150 nm height and 90 nm span	1.1×10^{-13}	3.02×10^{-13}	1.06×10^{-13}

Also, propagation length (L_{sp}) can be described in terms of an imaginary surface plasmon wave vector. The L_{sp} is calculated using equation no 2 given below.

$$L_{sp} = \frac{1}{2k''_x} \tag{2}$$

For Ag propagation length is larger so it absorbs less power therefore the SPP can propagate a large distance before it dies out. The penetration depth for metal and dielectric is given byequation 3.

$$\delta_s = \frac{\lambda_0}{2\pi \sqrt{\frac{\varepsilon_s + \varepsilon_m}{\varepsilon_m^2}}} \text{ and } \delta_s = \frac{\lambda_0}{2\pi \sqrt{\frac{\varepsilon_s + \varepsilon_m}{\varepsilon_m^2}}} \tag{3}$$

The penetration depth is larger in dielectric and smaller in metal due to the absorptive nature of metal. Since it is an absorptive field, it dies out quickly in metal. Also by performing the angular or spectral interrogation light inside the active layer can be trapped more efficiently which results in improved efficiency of TFSC.

Additionally, to determine the absorption, scattering, and extinction of spherical nanoparticles Mie theory has been employed [18, 19]. The scattering cross-section can be expressed as by equation 4

$$\sigma_{scat} = \frac{2\pi}{k^2} \sum_{n=1}^{\infty} (2n+1)\left(|a_n|^2 + |b_n|^2\right) \text{ and } \sigma_{ext} = \frac{2\pi}{k^2} Re(a_n + b_n) \tag{4}$$

where R is the radius of the nanosphere, K is the vacuum number of the incident light and p and m are the dielectric function of the nanosphere and medium.

The coefficient a_n and b_n can be calculated from the following equation 5

$$a_n = \frac{m\Psi_n(mx)\Psi_n(x) - \Psi_n(mx)\Psi'_n(x)}{m\Psi'_n(mx)\xi_n(x) - \Psi_n(mx)\xi'_n(x)}$$

and

$$b_n = \frac{\Psi'_n(mx)\Psi_n(x) - m\Psi_n(mx)\Psi'_n(x)}{\Psi'_n(mx)\xi_n(x) - m\Psi_n(mx)\xi'_n(x)} \tag{5}$$

Here, x is the size parameter, m is the square root ratio of the dielectric function of sphere and medium. Also, ψ, ξ are the Ricatti - Bessel cylindrical function of order n and differentiation, and ψ' and ξ' indicate differentiation with respect to argument x.

As the extinction cross-section is the summation of absorbed and scattered cross-section therefore absorption cross-section can be expressed by equation 6

$$\sigma_{abs} = \sigma_{ext} - \sigma_{scat} \tag{6}$$

We utilized equations (4)–(6) to determine the absorption cross-section of the spherical-shaped nanoparticles. However, we cannot determine the absorption cross-section of the pyramid-shaped nanoparticle. To address such limitations we performed FDTD simulation using Lumerical software. We have observed the absorption cross-section of differently shaped nanoparticles to get a general idea of the absorption pattern. We have noticed a significant improvement in the absorption pattern with an increment of the curvature of the nanoparticles. The following table summarizes the absorption cross-sections of different nanoparticles.

In table-1 we have taken the scattering cross-sections for three different wavelengths of the spectrum. This gives a better understanding of the absorption characteristics of different structures. From the table, we see that the absorption increases when the structure has a comparatively sharper edge. Edge sharpness increases gradually when the structure is changed as follows: nanospheres, nanorods, nanocubes, and nanopyramids. Since nanopyramids have a better absorption profile, we used them for our model of the solar cell.

In this paper, we performed optical and electrical simulations using FDTD to determine the key performance parameter such as absorption power (Pabs), generation rate (g), short circuit current density (J_{sc}) quantum efficiency of a solar cell QE (λ), photovoltaic efficiency (η), F is the fill-factor, and open-circuit voltage (V_{OC}) [20].
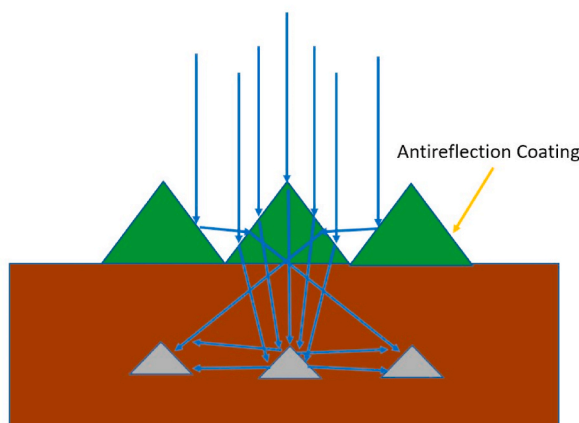
Fig. 1. Geometry for capturing light in thin-film plasmonic solar cells.

Light trapping of thin film solar cells: In solar cells, absorption coefficient and optical path length determine the amount of light absorbed by a semiconductor. However, some of the incoming light is reflected due to differences in the dielectric environment of the solar cell's interfaces. To increase the effective path length of light, various techniques such as texturing the top surface like a pyramid or introducing a rear mirror can be used.

The normal AM1.5 sun spectrum cannot be absorbed by conventional photovoltaic absorbers, which mainly lie in the spectral range of 600 nm–1100 nm. As a result, crystalline Si solar cells (wafer-based), which are conventional, typically have a larger thickness of 180–300 µm. To ensure that high-efficiency solar cells collect all photo carriers, the thickness of the material should be the diffusion lengths of the minority carrier. This is easily achievable for thin films, but it's difficult for thick films.

Fig. 1 shows the mechanism that is used in our solar cell model for increasing light absorption. When light falls on the pyramid-shaped antireflection coating, the light is focused on the pyramid-shaped nanoparticles inside the solar cell. Surface plasmon resonance occurs inside the solar cells and the light path is greatly increased.

The antireflection TiO2 pyramids' function is to direct light waves toward the silver pyramids inside the absorption layer. The periodicity and height of the pyramids are 720 nm and 550 nm respectively. These pyramids The periodicity of silver nanopyramids inside the absorption layer is determined by the upper antireflection pyramids' periods since each TiO_2 pyramid focuses light on a particular nanopyramid inside the absorption layer. This period has been selected after careful investigation of the generated photocurrent using simulations. When the period is decreased, the density of silver pyramids increases creating disturbances in the collection of generated photocurrents. Even if decreasing the periodicity led to increased electron-hole pair formation, the net photocurrent would be reduced due to the recombination of electron-hole pairs at the silver-silicon interface. Furthermore, we are unable to significantly lower the periodicity since it must be commensurate with the wavelength of the incoming wave. On the other hand, we cannot increase the periodicity since doing so would decrease the electron-hole pair generation. We have chosen the period to be 720 nm considering these criteria and simulation results also agree with the ideas discussed above. The use of pyramid-shaped antireflection coating is polarization independent and does not depend on the proper orientation of the solar cell. Both TE and TM modes work perfectly with this setup. The interaction of the TE mode with the structure causes the light to be directed mostly along the surface of the pyramid and enter into the absorption layer. As a result, the optical path length increases, and the incident light's reflection decreases. The interaction between the structure and the TM mode of light results in a few waves being scattered in the horizontal directions and getting absorbed in the nearby pyramids. As a result, the incident light is reflected less, and the active layer of the solar cell absorbs more light.

The practical fabrication of this device can be realized using the transfer process at high temperatures (~200 °C) as discussed in Ref. [47]. Development of the silicon layer on the substrate can be conducted using the Helianthos method [48]. Fabrication of nano-pyramids follows the interference lithography process as discussed in Ref. [49]. The TiO_2 periodic array can be fabricated using soft imprint lithography [50]. Thus the total fabrication process follows some well-known manufacturing techniques and should not create much trouble for practical realization.

Modeling and simulation: In this study, we have created five different configurations, and the details of the structure are discussed below.

1 **TFSC-A:** This structure (Fig. 2a) is composed of the Si active layer. In addition, two short Aluminum junctions are integrated. The dimensions of the upper collecting junctions is as follows: length = 2 µm and thickness = 100 nm. The lower collecting junction covers the whole bottom portion of the silicon active layer and works as a reflecting layer. This model does not have any anti-reflective layer; instead, there are two protective layers, one at the top and the other at the bottom. The protective layers are composed of silica, and SiO_2, which also acts as an anti-reflective layer.
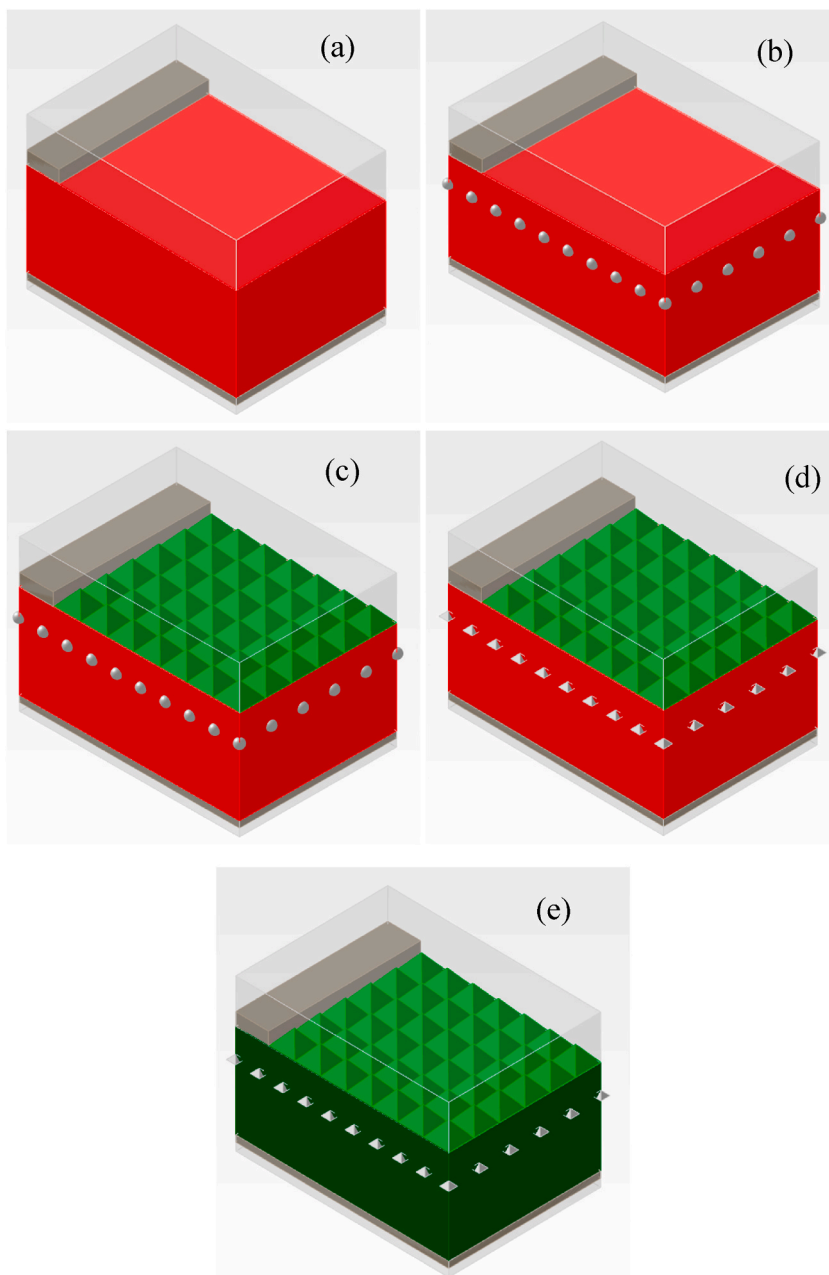
Fig. 2. The perspective view of TFSC. a) Composed of the Si active layer, with two aluminum junctions and SiO2 as a protective layer. b) Similar to TFSC-B, instead a silver nanosphere of 50 nm radius with a spacing of 360 nm was embedded within the absorption layer (Si). c) An additional anti-reflective layer composed of pyramid-shaped TiO2 was added with TFSC-B. d) The absorption layer was embedded with pyramid-shaped nano-particles instead of spherical nanoparticles, but other layers are similar to TFSC-C. e) Inp was used as the absorption layer instead of Si. Pyramid-shaped TiO2 is used as an antireflective layer and the SiO2 layer as a protective layer.

2 TFSC-B: In this structure (Figure.2b), we have used regularly spaced silver nanospheres inside the silicon layer to increase the absorption efficiency. We simulated different spacings and radii of the nanospheres and obtained the best absorption for the spacing of 360 nm and the radius of 50 nm. The dimension of the Aluminum junctions is the same as the previous structure.

3 TFSC-C: The TFSC-C (Figure.2c) has an additional anti-reflective layer compared to TFSC-A. The anti-reflective layer is composed of pyramid-shaped TiO2 as depicted by the green color. This layer minimizes the reflection of the incoming light and thus increases absorption.

4 TFSC-D: In this structure (Figure.2d), we have replaced the silver nanospheres with pyramid structures. The width of the lower portion of the structure is 300 nm and the height is 150 nm. The spacings between the nano-pyramids are the same as the spacings
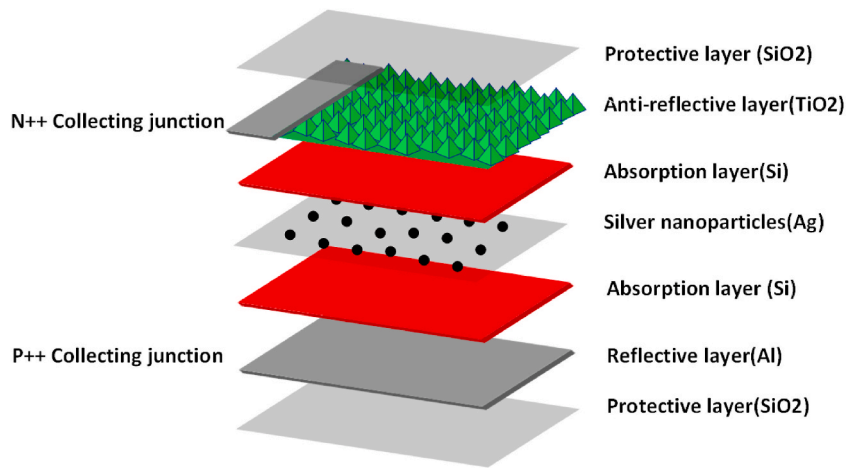
Fig. 3. Perspective view of TFSC showing each layer. Silver nanoparticles are embedded within the absorption layer (Si). Also on top of that TiO2 anti-reflective layer and at the bottom Al as a reflective layer was used.

Table-2
Thickness of different layers.

Layers	Thickness (nm)
Anti-reflecting Layer (TiO2)	550
Absorption Layer (upper part)	600
Silver Nanoparticles	150
Absorption Layer (lower part)	2250
Reflective Layer	200
Protective Layer	500
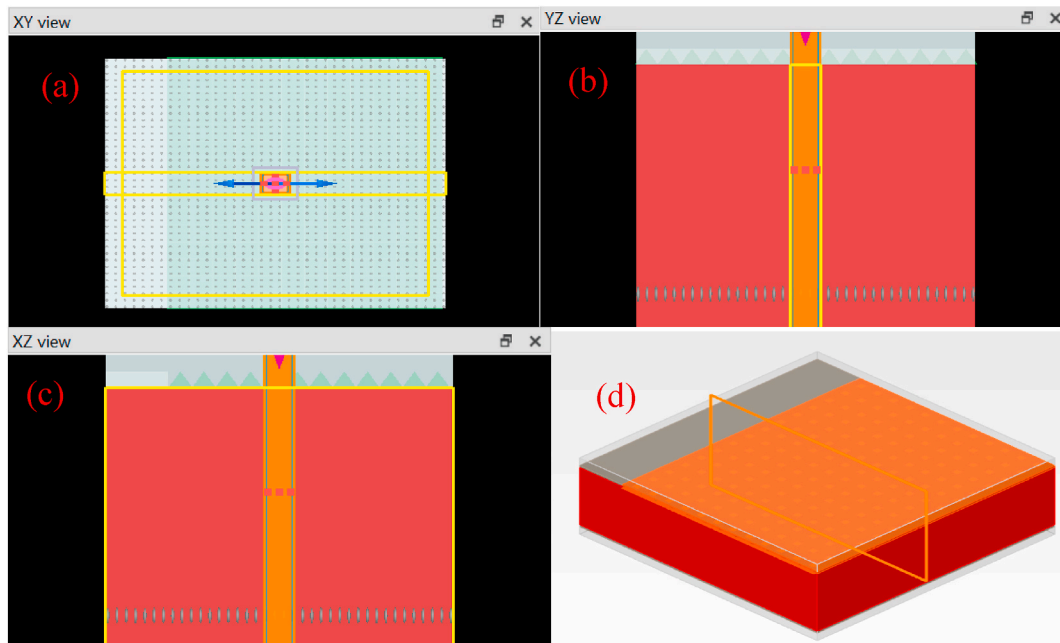
Fig. 4. 2D perspective view of FDTD and device simulation. Fig.4. a-c) XY, XZ and YZ view of the model in FDTD. Fig. 4d) The perspective view of the model in CHARGE.
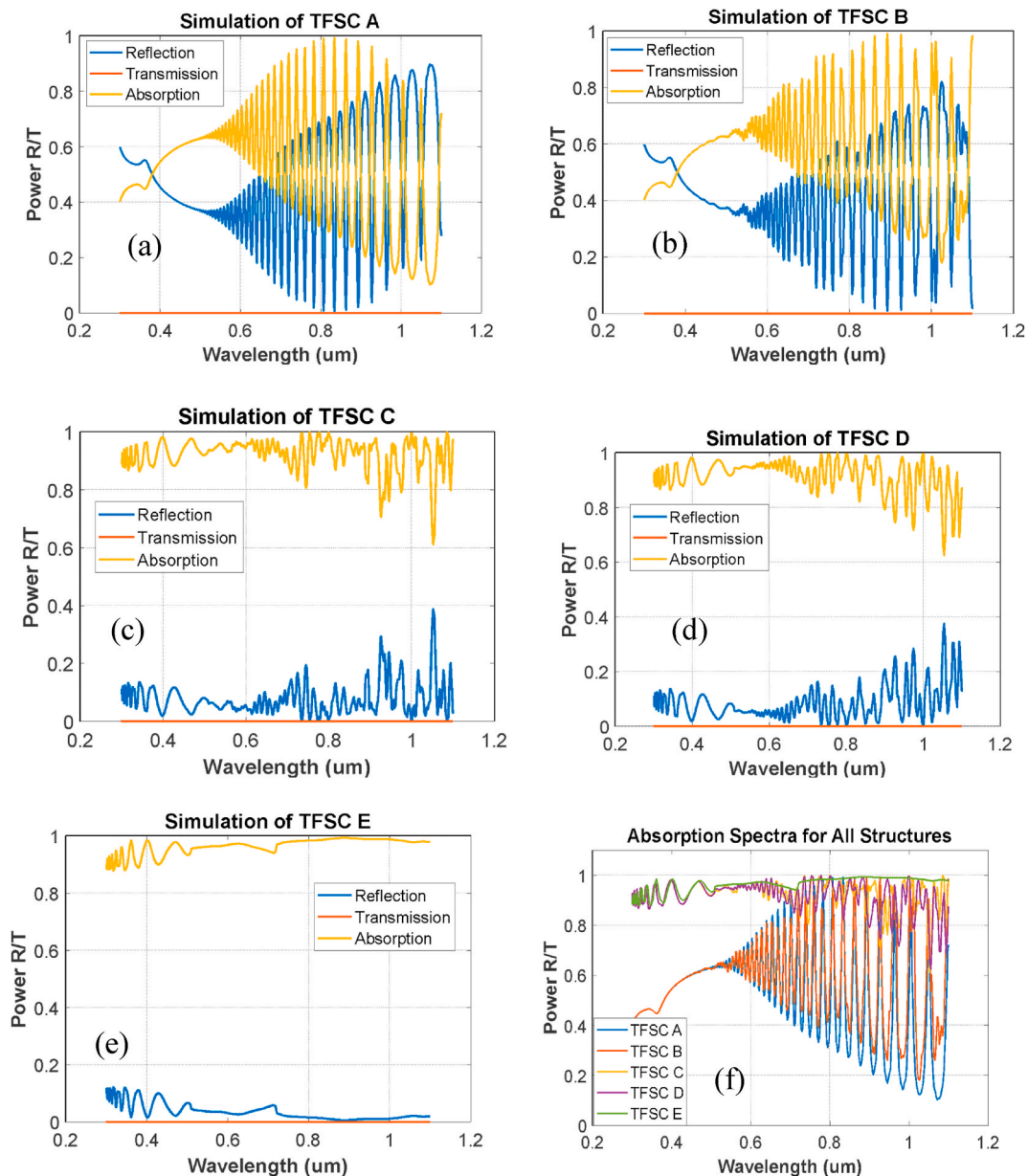
Fig. 5. Reflection, Transmission, and Absorption Spectrum for TFSC (a) A, (b) B, (c) C, (d) D, (e) E. Here transmission is almost zero for all cases. (f) Absorption spectra for all structures.

between the nanospheres (360 nm). These dimensions were chosen after a detailed sweep of the parameters. These pyramid structures can manipulate the incoming light better than nanospheres and thus increase absorption.

5 TFSC-E: We have replaced the absorption layer of the solar cell in this structure (Figure.2e). The silicon layer has been replaced by the InP layer keeping the thickness or doping profile constant. The introduction of InP effectively increases light absorption because of being a direct band gap material.

The perspective view of the final model is shown in Fig. 3. The model includes 4 different layers; the protective (light gray), the anti-reflective (green), the absorption (red), and the reflective (gray) layers (Fig. 2). In between the Si absorptive layer (thickness = 3 μm), we embedded a pyramid-shaped silver (Ag) nanoparticle array which enables surface plasmon and enhances absorption efficiency. On top of the absorption layer, there is a pyramid-shaped anti-reflecting layer made of TiO$_2$ which reduces reflection loss. Below the absorption layer, there is an aluminum (Al) reflective layer of a thickness of 200 nm, that enhances the absorption. At the top and bottom, there is a protective layer composed of silica and SiO$_2$ with a thickness = 500 nm which prevents surface contamination and oxidation. The thickness of different layers is summarized in Table 2.
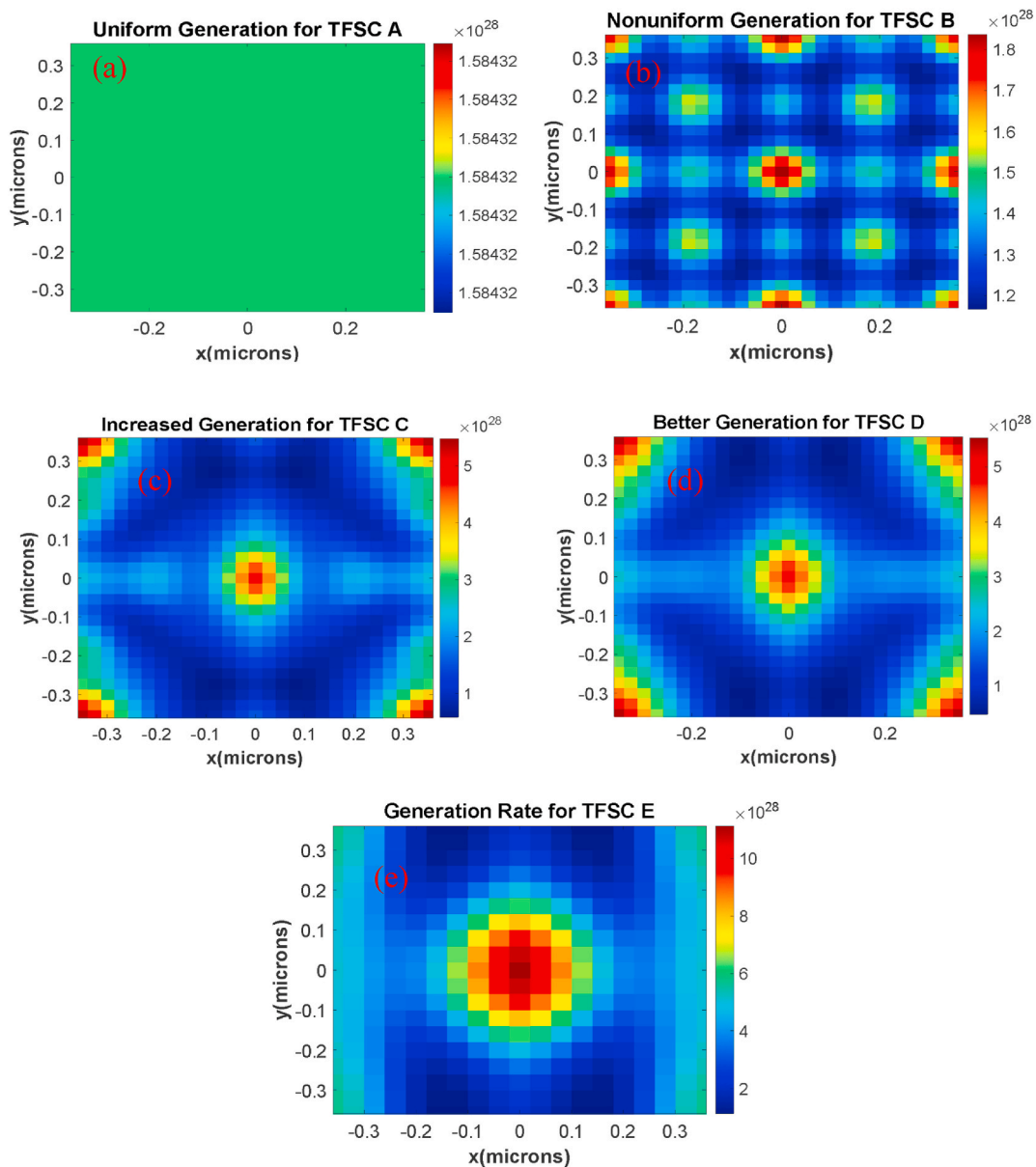
Fig. 6. Solar generation rate for TFSC (a) A, (b) b, (c) c, (d) d, (e) e.

Modeling in FDTD and CHARGE: Absorption per unit volume (P_{abs}), generation rate (g), and quantum efficiency (QE) are calculated from the optical simulation (FDTD). From the electrical simulation (CHARGE), short circuit current (I_{sc}), open circuit voltage (V_{oc}), fill factor (FF) and finally photovoltaic energy conversion efficiency, η are determined.

Prior to the fabrication of the model, simulation is necessary to analyze the optical profiles and electrical parameters. Fig. 4(a–d) shows the corresponding setup for optical and electrical simulations. As we incorporate more layers composed of different materials, the geometry of the model becomes complex. Thus, it becomes challenging to find an appropriate analytical method.

Optical simulation has been obtained using the FDTD method which solves Maxwell's equations. In the simulation, a plane wave with TE-mode was used as source (propagation direction in z backward axis), FDTD simulation area, a couple of mesh override regions, and transmission and reflection monitors were set. The highest mesh step was $dx = 20$ nm, $dy = 20$ nm, and $dz = 20$ nm. The FDTD calculates the generation rate and Pabs in the active layer. However, the number of electron and hole pairs at the P++ and N++ junctions was determined by the Charge solver using a finite-element method (FEM).
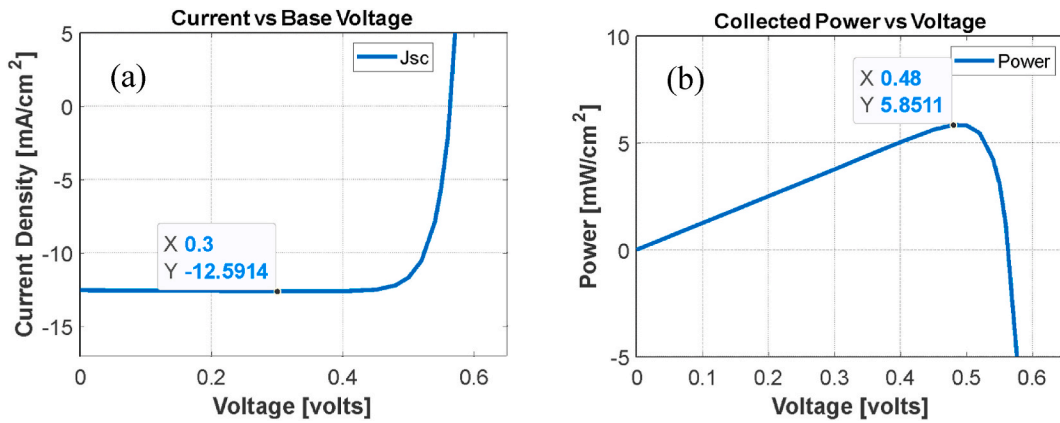
Fig. 7. Device solver (a) Current density J_{sc} vs. Voltage (V) relation (b) Power (P) vs. Voltage (V) relation for TFSC-A.

3. Results and discussion

Results from the optical simulation: From our simulation, we obtained absorption (A), transmission (T), and reflection (R) curves for five different models TFSC-A, B, C, D, and E correspondingly. Maxwell equations were solved using the FDTD method. With the aid of the solution, reflection, and transmission spectra were obtained. In the simulation, total reflected power and total transmitted power were measured using two frequency-domain power monitors. On the other hand, the total absorption was calculated using the following equation no 7:

$$A(\lambda) = 1 - R(\lambda) - T(\lambda) \tag{7}$$

TFSC-A: From 400 to 600 nm wavelength (λ), the total absorbed power ranges between 0.60 (a.u) and 0.90 (a.u) approximately (Fig. 5a). At wavelengths outside this range, fluctuation is observed, and the absorption decreases significantly reaching 0.06072 (a. u.). The maximum absorbed power is 0.9933 (a.u) at $\lambda = 833$ nm. The spectrum for the total reflected power is the mirror image of the absorption spectrum because the transmission is zero for all wavelengths. The minimum reflected power is very close to zero, near 833 nm. The J_{sc} value is 21.0575 mA/cm^2. The electron-hole generation graph is uniform (Fig. 6a).

TFSC-B: No fluctuation is observed before 510 nm (Fig. 5b). Outside this range, the curves for total absorbed power and total reflected power are seen to oscillate intensely. These curves are a mirror image of each other. Between the 400–600 nm spectral range, the total absorbed power ranges from 0.40 (a.u) to 0.70 (a.u) approximately with a maximum power of 0.99 (a.u) at $\lambda = 889$ nm. From the generation rate figure (Fig. 6b), we see that there is higher absorption in the middle of the figure. The reason for this increased absorption is the presence of spherical nanoparticles. The Jsc value is increased to 25.6083 mA/cm^2.

TFSC-C: We can see great improvement in the absorption spectra after the introduction of the anti-reflection layer. (Fig. 5c). The light is converted to the nano-spheres by the presence of the TiO$_2$ pyramids and consequently increases the light absorption. The absorption decreases to some extent after 900 nm. Maximum absorption is attained at 752 nm reaching a maximum value of 0.9901 (a. u.). From Fig. 6c, we see that the maximum generation is observed at the center of the figure, where the nanosphere is located. The Jsc value is further increased to 34.0752 mA/cm^2.

TFSC-D: The maximum absorption from silicon solar cells has been obtained by using silver nano-pyramids in place of nanospheres (Fig. 5d). Nanopyramids redirect light waves horizontally inside the silicon layer thus the absorption increases. The absorption is maximum in the range of 300 nm–900 nm. The generation rate graph (Fig. 6d) depicts the importance of nanopyramids. Light is mainly absorbed near the nanopyramids, and absorption gradually decreases away from it. The Jsc value is 37.1902 mA/cm^2 for this structure.

TFSC-E: This is our final proposed model. We have used the ideas from TFSC A-D about the effectiveness of different methods to improve efficiency. Finally, we have replaced the silicon layer for improvement in absorption. From Fig. 5e, we see a significant improvement in the absorption spectrum. The oscillations in the higher wavelengths are removed and we observe a flat line in this range. The reflection spectrum is also flat, and the value is relatively lower than the previous structures. The generation is improved (Fig. 6e).

The transmitted power is zero for all the above structures. The reflective Aluminum layer reflects light back to the absorbing silicon or InP layer and thus minimizes loss. We now plot the combined absorption spectra in Fig. 5f. The patterns of the spectra for TFSC A and B are almost similar. But the value of the absorption dips is less for TFSC B, which depicts the effect of introducing nanospheres into the solar cell. The absorption has further improved after using an anti-reflection layer in TFSC C. The maximum absorption is obtained with TFSC E, which has an almost flat absorption for all wavelengths.

Results from the electrical simulation: The effectiveness of a solar cell to produce electricity depends not only on the amount of absorbed light but the number of electron-hole pair generations (Fig. 6a–e). The electrons and holes must be effectively collected by the electrodes and brought out in the outer circuit for the current generation. The optical simulation is not capable of considering all the non-idealities while calculating the value of Jsc and thus we need electrical stimulation. The electrical simulation is performed using the CHARGE as already mentioned. Since the CHARGE solver considers all the non-idealities, the value of the current decreases to some
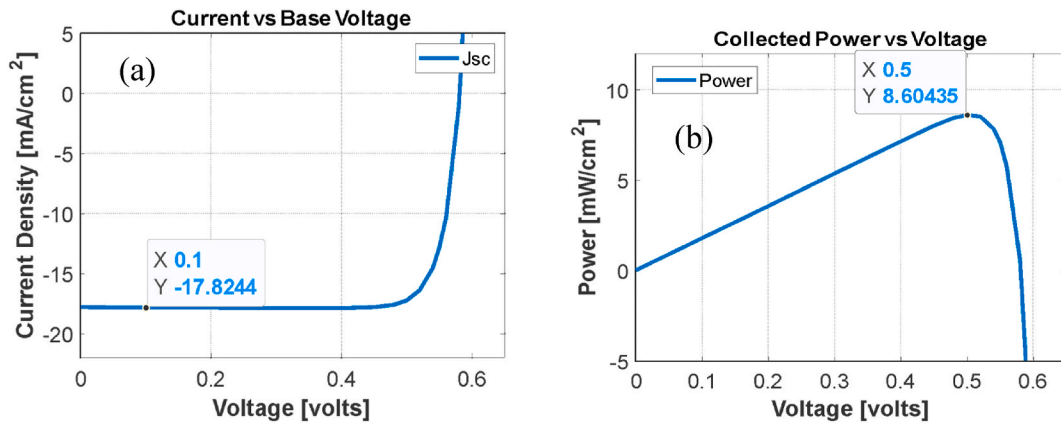
Fig. 8. Device solver (a) Current density J_{sc} vs. Voltage (V) relation (b) Power (P) vs. Voltage (V) relation for TFSC-B.
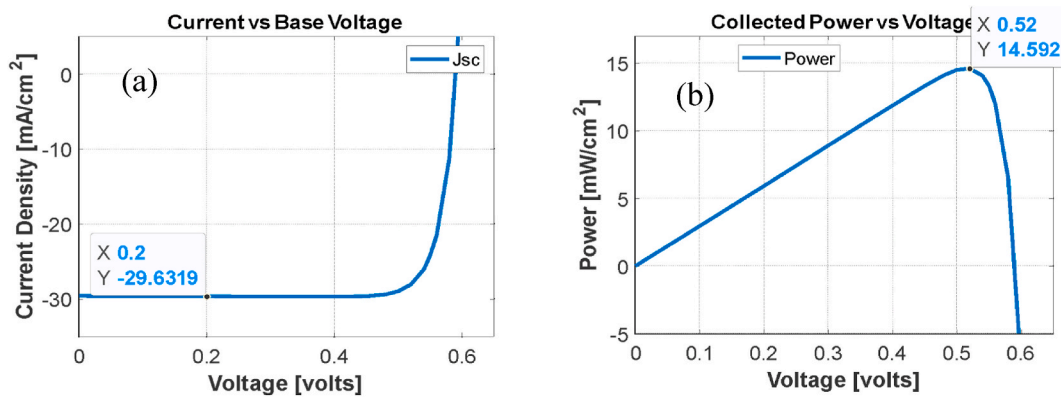

Fig. 9. Device solver (a) Current density J_{sc} vs. Voltage (V) (b) Power (P) vs. Voltage (V) relation for TFSC-C.
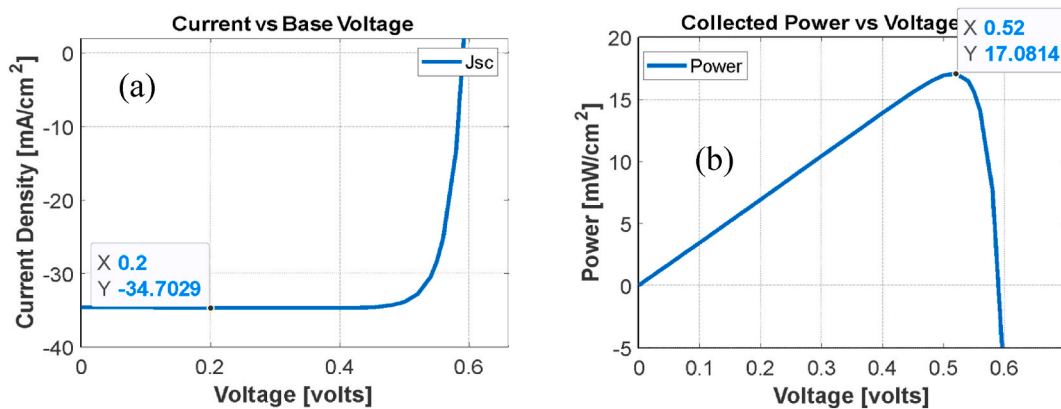

Fig. 10. Device solver (a) Current density J_{sc} vs. Voltage (V) (b) Power (P) vs. Voltage (V) relation for TFSC-D.

extent compared to the optical simulation results. From this section of the analysis, two graphs for each model of TFSCs were obtained. One graph shows the total power absorbed (P) against voltage (V) while the other is for current density (J_{sc}) against voltage (V). The power is observed to increase linearly with voltage. As the voltage goes nearer to 0.6 V, the curve is seen shifting to a negative slope followed by a drastic fall. On the contrary, the current density maintains a constant value with a horizontal line as the voltage increases. After crossing a certain voltage value, the curve shifts to a positive slope followed by a sharp increase. The same scenario is observed for each model.

TFSC-A: A number of electrical quantities are obtained. The open circuit voltage, $V_{oc} = 0.562$ V, and the short circuit current
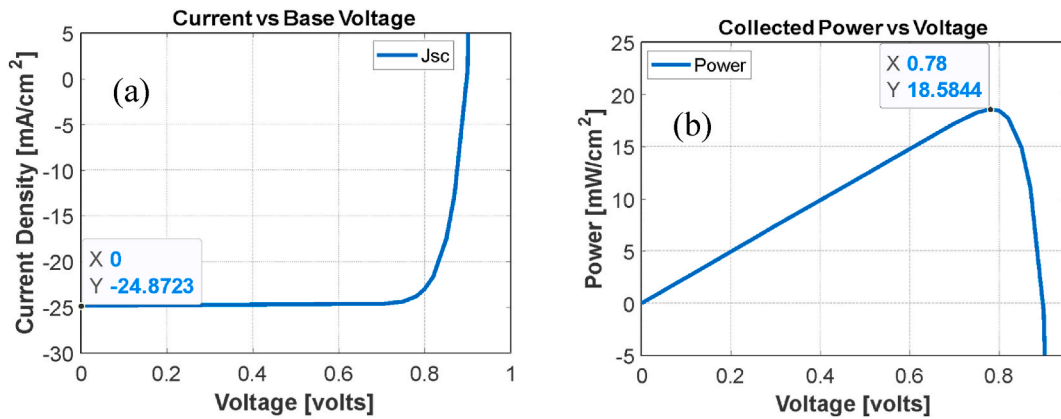
Fig. 11. Device solver (a) Current density J_{sc} vs. Voltage (V) relation; (b) Power (P) vs. Voltage (V) relation for TFSC-E.
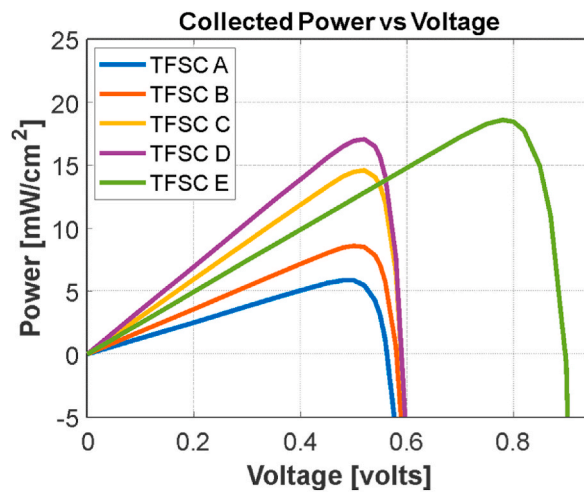

Fig. 12. Total absorbed power (P) vs. voltage (V) for all the structures.

Table-3
Charge Transport Solver-The electrical simulation results.

Structures	V_{OC} (V)	J_{SC} (mA/cm^2)	Pmax (mW/cm^2)	FF	%
TFSC-A	0.562	12.5914	5.8511	0.8269	5.8511
TFSC-B	0.581	17.8244	8.6044	0.8308	8.6044
TFSC-C	0.583	29.6319	14.592	0.8447	14.592
TFSC-D	**0.584**	**34.7029**	**17.0814**	**0.8428**	**17.0814**
TFSC-E	**0.923**	**24.8723**	**18.5844**	**0.8095**	**18.5844**

density, $J_{sc} = 12.5914 \, mA/cm^2$. The maximum power absorbed, $P_{max} = 5.8511 \, mW/cm^2$, and the fill factor, FF = 0.8269. Finally, the overall efficiency is obtained as 5.8511% (Fig. 7a and b), which is very low.

TFSC-B: The open circuit voltage, $V_{oc} = 0.581$ V, and the short circuit current density, $J_{sc} = 17.8244 \, mA/cm^2$. The maximum power absorbed, $P_{max} = 8.60435 \, mW/cm^2$ and the fill factor, FF = 0.83085. Finally, the overall efficiency is obtained as 8.60435% (Fig. 8a and b).

TFSC-C: A number of electrical quantities are obtained. The open circuit voltage, $V_{oc} = 0.583$ V, and the short circuit current density, $J_{sc} = 29.6319 \, mA/cm^2$. The maximum power absorbed, $P_{max} = 14.592 \, mW/cm^2$ and the fill factor, FF = 0.8447. Finally, the overall efficiency is obtained as 14.592% (Fig. 9a and b).

TFSC-D: Further improvement in electrical properties is noticed in this structure. The open circuit voltage, $V_{oc} = 0.584$ V, and the short circuit current density, $J_{sc} = 34.7029 \, mA/cm^2$. The maximum power absorbed, $P_{max} = 17.0814 \, mW/cm^2$, and the fill factor, FF = 0.8428. Finally, the overall efficiency is obtained as 17.0814% (Fig. 10a and b).

TFSC-E: The open circuit voltage increases significantly at this configuration, but Jsc decreases. Here, $V_{oc} = 0.923$ V and the short

Table- 4
Device Solver: Dopant concentrations of TFSCs.

Properties	Pepi	Anode (Base) back diff (p++)	Cathode (Emitter) nwell (n++)
xmin (μm)	−3	−2.2	−0.9
xmax (μm)	13	12.2	1.9
ymin (μm)	−6	−5	−5
ymax (μm)	6	5	5
zmin (μm)	−4	−3	−0.4
zmax (μm)	2	−2.8	0
Dopant type	p	p	n
Source face	All domains	Lower z	Upper z
Junction width (μm)	–	0.2	0.4
Distribution function	–	erfc	erfc
Concentration (cm^{-3})	2×10^{16}	10^{19}	10^{19}
Ref. concentration (cm^{-3})	–	10^{10}	10^{10}

circuit current density, J_{sc} = 24.8723 mA/cm^2. The maximum power absorbed, P_{max} = 18.5844 mW/cm^{2,} and the fill factor, FF = 0.8095. Finally, the overall efficiency is obtained as 18.5844% (Fig. 11a and b).

We have arranged the total power for all the models in one plot. This allowed for a better comparison among the obtained curves. From the graph, it can be concluded that the maximum value for power is obtained for our finally proposed model TFSC-E. The P_{max} = 18.5844 mW/cm^2 (Fig. 12).

The overall results and outcomes have been jotted down in the following Table 3. The five electrical quantities that have been obtained from the five models are V_{oc}, J_{sc}, P_{max}, FF, and % efficiency. The table depicts that, with every model the values of the parameters increase; TFSC-E having the highest values compared to the other models.

The reason for performing this study is to obtain better efficiency compared to state-of-the-earth technologies. According to previous studies, the maximum efficiency obtained from thin film solar cells using spherical nanoparticles is 16% [7,8]. Our work surpassed that efficiency by a good margin (17.0814%). We have obtained further improvement using InP as the solar cell medium. The correlation between all the structures is summarized in the following table.

As the thin film solar cells are under study, initially we defined its space charge-region. The background doping concentration of silicon was set to 2×10^{16}. This was followed by the specification of two other diffusion regions for n-type and p-type dopant concentration under the anode and cathode respectively. The rest has been displayed in the following Table 4.

4. Conclusion and future work

To conclude, we have demonstrated a thin-film solar cell where a pyramid-shaped silver nanoparticle array has been embedded between an active layer of silicon (Si) and InP. A pyramid-shaped anti-reflecting layer made of TiO$_2$, Al reflective layer, and SiO$_2$ protective layer has also been introduced which enables the LSPR excitations. The result from the CHARGE solver reveals that the silicon-based TFSC-D has a fill factor of 0.8428 with a power conversion efficiency of 17.08% and InP-based TFSC-E has a fill-factor of 0.8095 with a power conversion efficiency of 18.5844%. The previously reported maximum efficiency in thin-film solar cells using plasmonic nanoparticles is no more than 16.23% indicating that our model is at least 5% more efficient compared to the state-of-the-earth thin-film solar cells. Finally, we may state that this study summarizes the effect of silver pyramid-shaped nanoparticles, which is a noble plasmonic nanomaterial, inside the thin-film solar cells and obtains greater efficiency than the previously reported thin-film solar cells.

Author contribution statement

Abu S. M. Mohsin: Conceived and designed the experiments; Performed the experiments; Analyzed and interpreted the data; Contributed reagents, materials, analysis tools or data; Wrote the paper.

Sujoy Mondal: Performed the experiments; Analyzed and interpreted the data; Wrote the paper.

Monica Mobashera: Afrida Malik: Maliha Islam: Maisha Rubaiat: Performed the experiments; Analyzed and interpreted the data.

Data availability statement

Data will be made available on request.

Declaration of competing interest

The authors declare no competing interests.

Acknowledgment

Authors would like to thank Brac University Bangladesh for the research support.

References

[1] A.V. Shah, H. Schade, Milan Vanecek, J. Meier, E. Vallat-Sauvain, N. Wyrsch, U. Kroll, C. Droz, J. Bailat, Thin-film silicon solar cell technology, Progress in photovoltaics: Research and Applications 12 (2-3) (2004) 113–142.

[2] Stuart R. Wenham, Applied Photovoltaics, Routledge, 2011.

[3] Sven Rühle, Tabulated values of the Shockley–Queisser limit for single junction solar cells, Sol. Energy 130 (2016) 139–147.

[4] M.A. Photovoltaics, Green Third Generation. "Advanced Solar Energy Conversion, Springer Series in Photonics, 2003.

[5] Seweryn Morawiec, Manuel J. Mendes, Francesco Priolo, Isodiana Crupi, Plasmonic nanostructures for light trapping in thin-film solar cells, Mater. Sci. Semicond. Process. 92 (2019) 10–18.

[6] Bhaskar Singh, Mohammed M. Shabat, Daniel M. Schaadt, Wide angle antireflection in metal nanoparticles embedded in a dielectric matrix for plasmonic solar cells, Prog. Photovoltaics Res. Appl. 28 (7) (2020) 682–690.

[7] Abu S.M. Mohsin,, Monica Mobashera, Afrida Malik, Maisha Rubaiat, Maliha Islam, Light trapping in thin-film solar cells to enhance the absorption efficiency using FDTD simulation, J. Opt. 49 (2020) 523–532.

[8] Afsaneh Asgariyan Tabrizi, Pahlavan Ali, Efficiency improvement of a silicon-based thin-film solar cell using plasmonic silver nanoparticles and an antireflective layer, Opt Commun. 454 (2020), 124437.

[9] K.R. Catchpole, Polman Albert, Plasmonic solar cells, Opt Express 16 (26) (2008) 21793–21800.

[10] Hairen Tan, Rudi Santbergen, Arno HM. Smets, Miro Zeman, Plasmonic light trapping in thin-film silicon solar cells with improved self-assembled silver nanoparticles, Nano Lett. 12 (8) (2012) 4070–4076.

[11] Moritz Riede, Donato Spoltore, Karl Leo, Organic solar cells—the path to commercial success, Adv. Energy Mater. 11 (1) (2021), 2002653.

[12] Jingbo Zhao, Yunke Li, Guofang Yang, Kui Jiang, Haoran Lin, Harald Ade, Wei Ma, Yan He, Efficient organic solar cells processed from hydrocarbon solvents, Nat. Energy 1 (2) (2016) 1–7.

[13] Khushboo Sharma, Vinay Sharma, S.S. Sharma, Dye-sensitized solar cells: fundamentals and current status, Nanoscale Res. Lett. 13 (1) (2018) 1–46.

[14] I-Kang Ding, Zhu Jia, Wenshan Cai, Soo-Jin Moon, Ning Cai, Peng Wang, M. Shaik, Zakeeruddin, et al., Plasmonic dye-sensitized solar cells, Adv. Energy Mater. 1 (1) (2011) 52–57.

[15] Md K. Nazeeruddin, Etienne Baranoff, Michael Grätzel, Dye-sensitized solar cells: a brief overview, Sol. Energy 85 (6) (2011) 1172–1178.

[16] Muñoz García, Ana Belén, Iacopo Benesperi, Gerrit Boschloo, Javier J. Concepcion, Jared H. Delcamp, Elizabeth A. Gibson, J. Gerald, Meyer, et al., Dye-sensitized solar cells strike back, Chem. Soc. Rev. 50 (22) (2021) 12450–12550.

[17] Wei Liu, Hailing Ma, Annika Walsh, Advance in photonic crystal solar cells, Renew. Sustain. Energy Rev. 116 (2019), 109436.

[18] Junshi Liu, Mengnan Yao, Liang Shen, Third generation photovoltaic cells based on photonic crystals, J. Mater. Chem. C 7 (11) (2019) 3121–3145.

[19] K. Bergenek, Ch Wiesmann, R. Wirth, L. O'Faolain, N. Linder, K. Streubel, T.F. Krauss, Enhanced light extraction efficiency from AlGaInP thin-film light-emitting diodes with photonic crystals, Appl. Phys. Lett. 93 (4) (2008), 041105.

[20] S. Domínguez, I. Cornago, O. García, M. Ezquer, M.J. Rodríguez, A.R. Lagunas, J. Pérez-Conde, J. Bravo, Design, optimization and fabrication of 2D photonic crystals for solar cells, Photon. Nanostruct: Fundam. Appl. 11 (1) (2013) 29–36.

[21] Pierpaolo Spinelli, V.E. Ferry, J. Van de Groep, M. Van Lare, M.A. Verschuuren, R.E.I. Schropp, H.A. Atwater, A. Polman, Plasmonic light trapping in thin-film Si solar cells, J. Opt. 14 (2) (2012), 024002.

[22] Sourav Bose, J.M.V. Cunha, J. Borme, Wei-Chao Chen, N.S. Nilsson, J.P. Teixeira, J. Gaspar, et al., A morphological and electronic study of ultrathin rear passivated Cu (In, Ga) Se2 solar cells, Thin Solid Films 671 (2019) 77–84.

[23] N.P. Hylton, X.F. Li, V. Giannini, K.-H. Lee, N.J. Ekins-Daukes, Josine Loo, Dries Vercruysse, et al., Loss mitigation in plasmonic solar cells: aluminium nanoparticles for broadband photocurrent enhancements in GaAs photodiodes, Sci. Rep. 3 (1) (2013) 1–6.

[24] Traci R. Jensen, , Michelle Duval Malinsky, Christy L.Haynes, Richard P. Van Duyne, Nanosphere lithography: tunable localized surface plasmon resonance spectra of silver nanoparticles, J. Phys. Chem. B 104 (45) (2000) 10549–10556.

[25] Vincenzo Amendola, Roberto Pilot, Marco Frasconi, Onofrio M. Maragò, Maria Antonia Iatì, Surface plasmon resonance in gold nanoparticles: a review, J. Phys. Condens. Matter 29 (20) (2017), 203002.

[26] Ankush Kumar, Predicting efficiency of solar cells based on transparent conducting electrodes, J. Appl. Phys. 121 (1) (2017), 014502.

[27] Linxiao Zhu, Aaswath P. Raman, Shanhui Fan, Radiative cooling of solar absorbers using a visibly transparent photonic crystal thermal blackbody, Proc. Natl. Acad. Sci. USA 112 (40) (2015) 12282–12287.

[28] Mohsin, S.M. Abu, B. Mariam, Salim. "Probing the plasmon coupling, quantum yield, and effects of tip geometry of gold nanoparticles using analytical models and FDTD simulation." IEEE Photonics Journal 10 (3) (2018) 1–10.

[29] Abu S.M. Mohsin,, Aggregation and Uptake Kinetics of Gold Nanoparticles in Biological Cells, Using Plasmon Coupling and Image Correlation Spectroscopy, Swinburne University of Technology, Melbourne, 2015.

[30] Mohsin, S.M. Abu, B. Mariam, Salim. "Probing the intracellular refractive index and molecular interaction of gold nanoparticles in HeLa cells using single particle spectroscopy." International journal of nanomedicine 13 (2018) 6019.

[31] Y. Gassenbauer, K. Ramspeck, B. Bethmann, K. Dressler, J.D. Moschner, M. Fiedler, E. Brouwer, et al., Rear-surface passivation technology for crystalline silicon solar cells: a versatile process for mass production, IEEE J. Photovoltaics 3 (1) (2012) 125–130.

[32] J. Gee, How to Make Solar Panels More Efficient in 2018." EnergySage." EnergySage Solar News Feed, EnergySage 19 (2017).

[33] Adam B. Taylor, Pierrette Michaux, Abu SM. Mohsin, James WM. Chon, Electron-beam lithography of plasmonic nanorod arrays for multilayered optical storage, Opt Express 22 (11) (2014) 13234–13243.

[34] Seweryn Morawiec, Jakub Holovský, Manuel J. Mendes, Martin Müller, Kristina Ganzerová, Aliaksei Vetushka, Ledinský Martin, Francesco Priolo, Antonin Fejfar, Isodiana Crupi, Experimental quantification of useful and parasitic absorption of light in plasmon-enhanced thin silicon films for solar cell application, Sci. Rep. 6 (1) (2016), 22481.

[35] Claire ER. Disney, Supriya Pillai, Martin A. Green, The Impact of parasitic loss on solar cells with plasmonic nano-textured rear reflectors, Sci. Rep, 7 (1) (2017) 1–10.

[36] Christian S. Schuster, Morawiec Seweryn, Manuel J. Mendes, Patrini Maddalena, R.Martins Emiliano, Lewis Liam, Isodiana Crupi, Thomas F. Krauss, Plasmonic and diffractive nanostructures for light trapping—an experimental comparison, Optica 2 (3) (2015) 194–200.

[37] Antonella Gentile, Francesco Ruffino, Maria Grazia Grimaldi, Complex-morphology metal-based nanostructures: fabrication, characterization, and applications, Nanomaterials 6 (6) (2016) 110.

[38] Sahar Royanian, , Ali Abdolahzadeh Ziabari, Reza Yousefi, Efficiency enhancement of ultra-thin CIGS solar cells using bandgap grading and embedding Au plasmonic nanoparticles, Plasmonics 15 (4) (2020) 1173–1182.

[39] S. Phetsang, S. Anuthum, P. Mungkornasawakul, C. Lertvachirapaiboon, R. Ishikawa, K. Shinbo, K. Kato, K. Ounnunkad, A. Baba, Enhancement of organic thin-film solar cells by incorporating hybrid Au nanospheres and Au nanorods on a metallic grating surface, Molecular Crystals and Liquid Crystals 705 1 (2020) 41–47.

[40] R.J. Veenkamp, W.N. Ye, Plasmonic metal nanocubes for broadband light absorption enhancement in thin-film a-Si solar cells, J. Appl. Phys. 115 (12) (2014), 124317.

[41] Tahir Iqbal, Sayyam Ahsan, Faiza Saeed, , Muhammad Shehzad Sultan, Abeer A. AlObaid, Warad Ismail, Arslan Masood, Improved efficiency of MoS2-Au Multilayer plasmonic-based solar cells: far-and near-field analysis, Plasmonics (2023) 1–11.

[42] Jing Rao, Sergey Varlamov, Light trapping in thin film polycrystalline silicon solar cell using diffractive gratings, Energy Proc. 33 (2013) 129–136.

[43] Ragip A. Pala, Justin White, Edward Barnard, John Liu, L. Mark, Brongersma, Design of plasmonic thin-film solar cells with broadband absorption enhancements, Adv. Mater. 21 (34) (2009) 3504–3509.

[44] Tahir Iqbal, Mohsin Ijaz, Muhammad Javaid, Muhammad Rafique, Khalid Nadeem Riaz, Muhammad Bilal Tahir, Ghulam Nabi, Muhammad Abrar, Sumera Afsheen, An optimal Au grating structure for light absorption in amorphous silicon thin film solar cell, Plasmonics 14 (2019) 147–154.

[45] Chunxue Ji, Liu Wen, Yidi Bao, Xiaoling Chen, Guiqiang Yang, Bo Wei, Fuhua Yang, Xiaodong Wang, Recent applications of antireflection coatings in solar cells, Multidisciplinary Digital Publishing Institute, Photonics 9 (12) (2022) 906.

[46] Harry A. Atwater, Polman Albert, Plasmonics for improved photovoltaic devices, Nat. Mater. 9 (3) (2010) 205–213.

[47] J.K. Rath, M. Brinza, Y. Liu, A. Borreman, R.E.I. Schropp, Fabrication of thin film silicon solar cells on plastic substrate by very high frequency PECVD, Solar Energy Materials and Solar Cells 94 9 (2010) 1534–1541.

[48] E. Middelman, E. Van Andel, R.E.I. Schropp, L.V. de Jonge-Meschaninova, P.G.M.G. Peters, R.J. Severens, H. Meiling, et al., New temporary superstrate process for roll-to-roll production of thin film solar cells, in: 2nd World Conference on Photovoltaic Solar Energy Conversion, 1998.

[49] Anastassios Mavrokefalos, Sang Eon Han, Selcuk Yerci, Matthew S. Branham, Gang Chen, Efficient light trapping in inverted nanopyramid thin crystalline silicon membranes for solar cell applications, Nano Lett. 12 (6) (2012) 2792–2796.

[50] Wei Jiang, Hongzhong Liu, Lei Yin, Yongsheng Shi, Bangdao Chen, Enhanced photoelectric properties in dye-sensitized solar cells using TiO2 pyramid arrays, J. Phys. Chem. C 120 (18) (2016) 9678–9684.